CrossMark

Exchange Bias Enhancement and Magnetic Proximity Effect in $FeVO_4$-Fe_3O_4 Nanoparticles

EHAB ABDELHAMID,[1] SUVRA S. LAHA,[1] AMBESH DIXIT,[2]
GHOLAM ABBAS NAZRI,[3] ONATTU D. JAYAKUMAR,[4]
and BORIS NADGORNY [ORCID][1,5]

1.—Department of Physics and Astronomy, Wayne State University, Detroit, MI 48201, USA.
2.—Department of Physics, Indian Institute of Technology Jodhpur, Rajasthan 342037, India.
3.—Department of Electrical and Computer Engineering, Wayne State University, Detroit, MI 48202, USA. 4.—Chemistry Division, Bhabha Atomic Research Centre, Mumbai 400085, India. 5.—e-mail: boris_nadgorny@wayne.edu

We study the behavior of the exchange bias (EB) and the blocking temperature in an antiferromagnetic $FeVO_4$–ferrimagnetic Fe_3O_4 nanocomposite system upon annealing in Ar atmosphere. Surprisingly, the blocking temperature of post-annealed samples increased to ~ 50 K, more than two-fold compared the Néel temperature ($T_N = 22$ K) of individual $FeVO_4$ nanoparticles. This significant enhancement of the blocking temperature was accompanied by the corresponding increase of EB, from ~ 50 Oe in as-prepared samples to ~ 110 Oe in post-annealed samples. The temperature dependence of EB can be described by two approximately linear regions with different slopes, with an inflection point at $T \sim 21$ K coinciding with the Néel temperature of $FeVO_4$ nanoparticles. The region above the inflection point with non-zero EB is characterized by a weaker temperature dependence and is expanded well beyond T_N. The x-ray photoemission spectroscopy measurements indicate that the surface of post-annealed Fe_3O_4 particles becomes oxygen deficient, which leads to a modification of the electronic, magnetic and morphological properties of the $FeVO_4/Fe_3O_4$ interface. We associate this unusual behavior with a magnetic proximity effect, in which the ordering temperature of the antiferromagnetic $FeVO_4$ nanoparticles and the corresponding exchange bias are strongly affected by the adjacent ferrimagnetic Fe_3O_4 layer.

Key words: Magnetic nanocomposites, exchange bias, Néel temperature

INTRODUCTION

Magnetic nanoparticle systems have been extensively investigated for understanding fundamental concepts in nanomagnetism[1–5] and exploring advanced biomedical applications.[6–10] Bi-component nanocomposites, and core–shell nanoparticle systems have gained considerable attention due to their high tunability and multifunctional properties, particularly those related to magnetic exchange-bias (EB),[11–14] a phenomenon observed at an interface between a ferromagnet/ferrimagnet (FM/FiM) and antiferromagnet (AFM) spin subsystems. The exchange coupling between interfacial AFM spins below the Néel temperature T_N and FM/FiM spins (with typically higher ordering/Curie temperatures) brings about a shift in magnetic hysteresis loops.[11,15,16] While the EB effect was discovered more than half a century ago[17] and has many important device applications, such as magnetic field sensors, read heads, and other spintronic devices,[15,18] the microscopic origin of EB is still not well understood,[11,19,20] particularly at the nanoscale,[21] where EB is largely determined by the

microscopic structure of the FM/AFM interface. While most studies of EB are performed in thin film structures, a number of core–shell nanoparticles and nanocomposite systems have been investigated, such as Co/Cr_2O_3,[11] Fe/Fe_3O_4,[12] FeO/Fe_3O_4,[13] $NiFe_2O_4/NiO$,[18] and MnO/Mn_3O_4.[22] Generally, EB vanishes at the so-called blocking temperature T_B; in an ideal case this temperature is equal to the Néel temperature of the antiferromagnetic phase transition, although experimentally it is often significantly lower than the Néel temperature due to the size-dependent exchange anisotropy.[23] From the application perspective, it is desirable to increase T_B; however, the increase of T_N does not automatically result in the corresponding enhancement of T_B, as has been demonstrated by van der Zaag et al. in the Fe_3O_4/CoO system,[21] where the authors attributed the increase of the Néel temperature in ultrathin CoO films to the magnetic coupling between the two magnetic systems and proximity to the ferrimagnetic Fe_3O_4. Similarly, Borchers et al. reported an increase in the ordering temperature of NiO thin films when coupled to Fe_3O_4.[24] On the other hand, the existence of considerable exchange-bias above the Néel temperature of the AFM phase of UO_2 has been reported by Tereshina et al.[25] in the case of UO_2/Fe_3O_4 thin films, where it was also argued that the effect was related to the proximity effect at the interface. Manna and Yusuf,[26] pointed to the interface exchange coupling as the common origin of both the exchange bias phenomenon and the magnetic proximity effect, which is probably why these two phenomena often occur simultaneously in the same system. Some recent experimental studies[27] point to spin frustration as a relevant factor in exchange anisotropy, resulting in the observed hysteresis loop shifts. Suggested spin frustration can be generated by frozen spins, forming a fraction of a monolayer and tightly locked to the AFM lattice, hence unable to rotate in an external magnetic field.[28] Frozen spins can also be locked within disordered spin glass layers,[29] which were found to contain substantial frustration, consistent with the presence of the exchange bias. These results point to the complex system-dependent origin of EB, particularly in nanostructured systems, where the role of interface is crucial and where the effective surface ordering temperature of the antiferromagnetic nanoparticles can be strongly affected by the adjacent ferromagnetic layers, such as in the case of Fe_xMn_{1-x}/Ni system.[30] In these cases, the temperature dependent studies of EB may be particularly important to reveal the nature of the interface effects.[31]

Here, we investigate the magnetic proximity effect in as-prepared and post-annealed $FeVO_4$-Fe_3O_4 nanocomposite AFM/FiM samples. We observed an anomalously high blocking temperature $T_B \sim 50$ K in post-annealed nanocomposites, compared to as-prepared samples in which T_B was found to be close to $T_{N1} = 22$ K, the transition temperature of a frustrated antiferromagnet $FeVO_4$ to a collinear AFM phase. This substantial increase of T_B is accompanied by the corresponding increase of the exchange bias values in the low temperature limit by approximately a factor of two. The XPS measurements suggest that the surface of thermally treated Fe_3O_4 is oxygen deficient, which may point to a possible mechanism of the observed blocking temperature enhancement beyond the Néel temperature of $FeVO_4$ nanoparticles.

EXPERIMENTAL PROCEDURES

The chemical co-precipitation technique was used to synthesize both $FeVO_4$ nanoparticles and $FeVO_4$-Fe_3O_4 nanocomposites. A solution of ammonium metavanadate (NH_4VO_3) in hot water was kept under reflux, to which iron nitrate ($Fe(NO_3)_3 \cdot 9H_2O$) dissolved in deionized water was added, in a 1:1 molar ratio. A light brown precipitate, formed at the end of the reaction (after 4 h), was collected and washed a few times with ethyl alcohol. The precipitate was then annealed in air for 4 h at 800°C to obtain $FeVO_4$ nanoparticles. The as-prepared $FeVO_4$ nanoparticles were then dispersed in deionized water and kept under continuous stirring at room temperature. To fabricate $FeVO_4$-Fe_3O_4 nanocomposites, an aqueous solution of $FeCl_3 \cdot 6H_2O$ and $FeCl_2 \cdot 4H_2O$ in a molar ratio of 2:1, was added to the dispersion, followed by dropwise addition of 1(M) NH_4OH. The formed precipitate was thoroughly washed to remove any residual basic ions and was then filtered and air-dried to obtain the desired nanocomposites. The as-prepared sample was then pressed into pellets and subjected to post-annealing treatment in argon gas at 400°C for 2 h. The as-prepared and post-annealed samples are referred to as sample A and sample B, respectively. The structural and morphological studies of the nanostructures were carried out using x-ray diffraction (Rigaku MiniFlex 600 x-ray diffractometer generating CuK_α radiation) and transmission electron microscopy (JEOL-2010 FasTEM operated at 200 kV), while the magnetic measurements were performed using the Quantum Design Physical Property Measurement System (PPMS®).

RESULTS AND DISCUSSION

The characteristic XRD patterns for both phase-pure $FeVO_4$ and $FeVO_4$-Fe_3O_4 nanocomposite samples (samples A and B) are shown in Fig. 1. All the peaks of the $FeVO_4$ sample (black) are indexed to phase-pure nanoparticles with a high degree of crystallinity and are in good agreement with JCPDS Card No: 38-1372. For samples A and B, the observed diffraction peaks correspond to the co-existence of two crystalline nanoparticle phases of $FeVO_4$ and Fe_3O_4 (JCPDS Card No: 85-1436), with some of the peaks from the two phases overlapping at a few locations (for example at 35.5°). The ($\bar{2}$20) and (311) indices, indicated in Fig. 1, correspond to
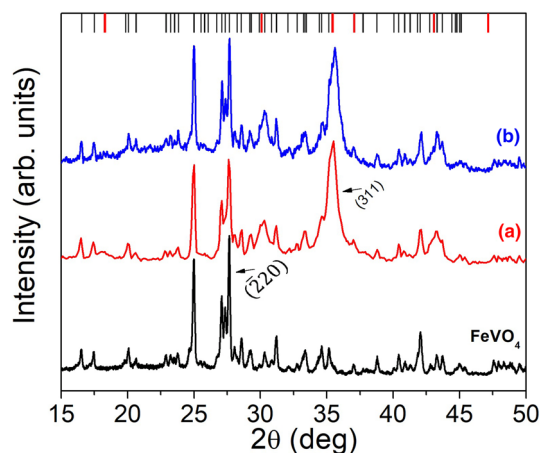
Fig. 1. XRD spectra of $FeVO_4$ (black), (a) as-prepared $FeVO_4$-Fe_3O_4 (red) and (b) argon annealed@400°C $FeVO_4$-Fe_3O_4 nanocomposites (blue). The standard peak locations of $FeVO_4$ (JCPDS card # 38-1372) and Fe_3O_4 (JCPDS card # 85-1436) are indicated by the top black and red marks respectively. The curves have been offset vertically for clarity. The (220) and (311) indices correspond to the most intense peaks of $FeVO_4$ and Fe_3O_4 respectively (Color figure online).

the most intense peaks of $FeVO_4$ and Fe_3O_4 respectively. Using the XRD spectra, we estimate the average crystallite sizes of $FeVO_4$ and Fe_3O_4 nanoparticles from the Scherrer equation. The average size of $FeVO_4$ and Fe_3O_4 nanoparticles in as-prepared samples was calculated to be 37 ± 4 nm and 11.8 ± 0.3 nm, respectively, whereas upon annealing the crystallite sizes of $FeVO_4$ and Fe_3O_4 nanoparticles became 40 ± 11 nm and 11.0 ± 0.6 nm, respectively. Somewhat surprisingly, the average crystallite size remained practically the same in post-annealed samples, although the particle size distribution, particularly of $FeVO_4$ nanoparticles, became less homogeneous after annealing. We also note that the isostructural character of magnetite Fe_3O_4 and maghemite (γ-Fe_2O_3) makes it difficult to directly and accurately identify these phases by using XRD alone. Mössbauer and XPS spectroscopy, on the other hand, allow precise identification of valence state of iron atoms and hence work best in distinguishing between magnetite and maghemite. In Fig. 2 below we will describe our XPS measurements, which allowed us to conclude that the ratio of Fe^{2+}/Fe^{3+} in as-prepared samples was equal to 33:67, as it should be for stoichiometric magnetite.

To probe the morphology and the nature of conglomeration between the two different types of nanoparticles, we have analyzed the nanocomposites using transmission electron microscopy (TEM). The TEM images and the respective energy dispersive spectroscopy (EDS) spectra of different regions of the argon-annealed nanocomposites (samples B) are shown in Fig. 3. Figure 3a clearly illustrates the agglomeration of both $FeVO_4$ and Fe_3O_4 nanoparticles, which is confirmed by the EDS spectrum shown in the inset. Figure 3b depicts a region of

clustered Fe_3O_4 nanoparticles, with the EDS data indicating almost complete absence of the vanadium peak. Two morphologically different types of particles have been identified; the larger particles are $FeVO_4$, while the smaller are Fe_3O_4, as shown in Fig. 3c. These microscopic measurements suggest that clusters of Fe_3O_4 nanoparticles surround $FeVO_4$ nanoparticles and are randomly adhered to the surface of $FeVO_4$. The TEM/EDS data allowed us to estimate the area of the interface between $FeVO_4$ and Fe_3O_4 nanoparticles as we will discuss below. At the same time, while the order of magnitude estimates of the Fe_3O_4 particles size from the TEM micrographs ($\sim$ 10–20 nm), seemed to be consistent with the numbers obtained from our XRD data, considerable particle clustering made it difficult to obtain reliable particle size statistics in order to evaluate the size of $FeVO_4$ nanoparticles from the TEM data.

The temperature and field dependent dc and ac magnetic properties of the nanocomposites were also analyzed. $FeVO_4$ is a frustrated antiferromagnet with a collinear AFM phase transitions at T_{N1} = 22 K and non-collinear AFM transition at T_{N2} = 15 K,[32] while Fe_3O_4 is FiM with T_C of about 850 K.[33] Figure 4 shows the real part of the normalized magnetic susceptibility χ'/χ'_{max} as a function of temperature for phase-pure $FeVO_4$ nanoparticles at 1 kHz in an excitation field of 10 Oe. Two frequency-independent features near 15 K and 22 K, indicated by the arrows, correspond to the two antiferromagnetic phase transitions of $FeVO_4$, in good agreement with the literature.[32,34,35] Figure 4 inset shows the imaginary part of the normalized magnetic susceptibility $\chi''/\chi''_{max.}$ as a function of temperature for as-prepared $FeVO_4$-Fe_3O_4 nanocomposites. The magnetic relaxation feature in the low temperature regime ($<$ 50 K), and the frequency dependent superparamagnetic blocking signature seen at approximately 200 K, is in line with the results obtained previously by Laha et at.[33,36,37] and by Long et al.[38] for Fe_3O_4 nanoparticles with the averages size of $\sim$ 11–12 nm, in good agreement with the average particle size estimates obtained here from the XRD data. It is to be noted that features associated with the antiferromagnetic phase transitions of $FeVO_4$, are likely to be overshadowed by the more prominent low-temperature relaxation feature of Fe_3O_4 nanoparticles resulting from structural defects.[33] We also note that our Fe_3O_4 nanoparticles do not display the Verwey transition, a signature feature of bulk magnetite, presumably due to their low crystallinity and small size ($\sim$ 10 nm), in agreement with the results in the literature.[39,40]

The exchange-bias measurements in the $FeVO_4$-Fe_3O_4 system were performed for both as-prepared and post-annealed nanocomposites, with the results shown in Fig. 5. Initially, the reference hysteresis loop (ZFC) was recorded at T = 5 K. Subsequently, the sample was allowed to cool down from
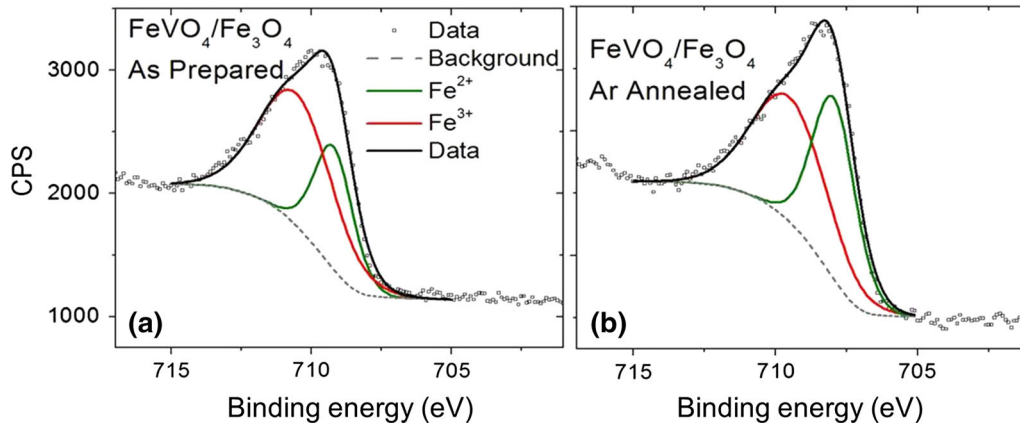
Fig. 2. XPS spectral line fits of the Fe ($2p^{3/2}$) line for (a) as-prepared (sample A) and (b) argon annealed $FeVO_4$-Fe_3O_4 nanocomposites (sample B). The Shirley background was subtracted, before fitting to a dual Gaussian–Lorentzian profile. The relative heights of the peaks give an estimate of the Fe^{2+}: Fe^{3+} ratio.

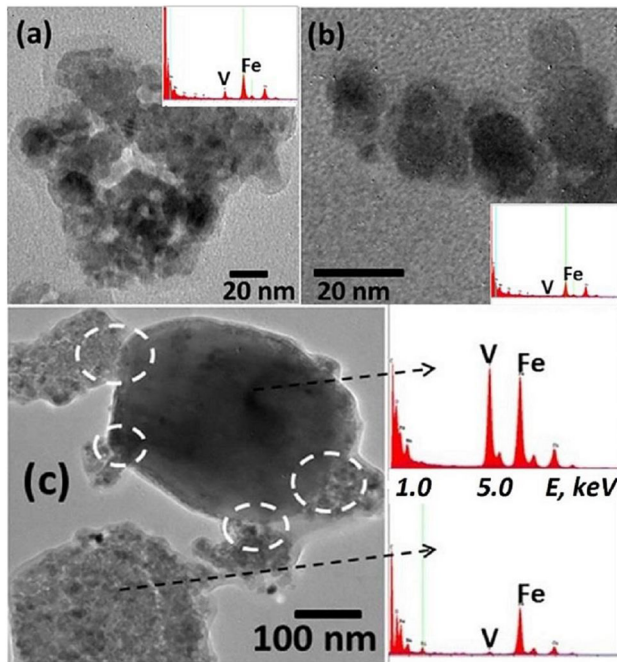Fig. 3. TEM images and EDS spectra of the argon annealed $FeVO_4$-Fe_3O_4 nanocomposites (Sample B); (a) region of agglomerated $FeVO_4$-Fe_3O_4 nanocomposites, with noticeable Fe and V peaks shown in the inset; (b) region of clustered Fe_3O_4 nanoparticles, inset indicating practically no vanadium peak present; (c) highlighted local interfaces of $FeVO_4$ and Fe_3O_4 nanoparticles (white circles), with the respective EDS spectra. The x-axis in the EDS spectra represents the binding energy in keV.
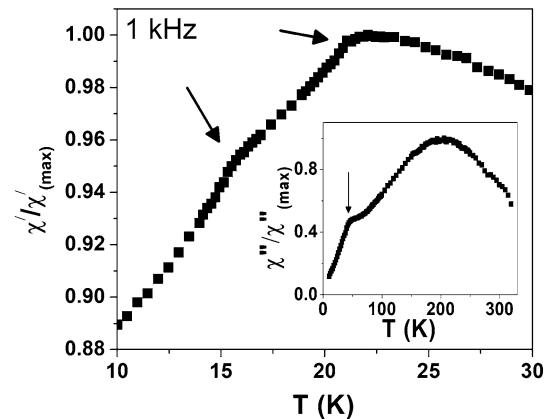

Fig. 4. $\chi'/\chi'_{max.}$ versus T plot for phase-pure $FeVO_4$ nanoparticles at $f = 1$ kHz. The inset shows $\chi''/\chi''_{max.}$ versus T behavior for the as-prepared $FeVO_4$-Fe_3O_4 nanocomposites (sample A). Note that features associated with the antiferromagnetic phase transitions of $FeVO_4$, are overshadowed by the more prominent low-temperature relaxation feature of Fe_3O_4 nanoparticles resulting from structural defects.

$T = 100$ K ($T_N < T < T_C$) to the desired temperature in the presence of a 2 T magnetic field (FC), after which the magnetization M versus H measurements were conducted. Figure 5a and b shows M/M_{max} versus H plots (both ZFC and FC) obtained using this procedure for as-prepared and post-annealed nanocomposites (samples A and B), respectively. The exchange field H_{exc} increased by approximately a factor of two; from $H_{exc} = 50$ Oe in as-prepared nanocomposites[13] to $H_{exc} = 110$ Oe in

argon annealed samples. The exchange bias in the post-annealed sample (sample B) decreased linearly with temperature, in agreement with the Malozemoff random-field model.[41] Moreover, quite unexpectedly, EB persisted well above the Néel temperature of $FeVO_4$ (see Fig. 6). This result is quite surprising, as in a typical AFM/FiM systems the blocking temperatures are lower that the corresponding Néel temperatures. The inflection point of the two intersecting linear regions of the plot in Fig. 6 corresponds to $T \sim 21$ K, which coincides with the Néel temperature of $FeVO_4$ nanoparticles. The region above the inflection point with non-zero EB is characterized by a weaker temperature dependence and expands well beyond T_N to ~ 50 K. Above 50 K, only a very small residual exchange bias, close to the accuracy of our magnetic measurements (1–2 Oe) may be present. The observed dependence is reminiscent to the one recorded in the
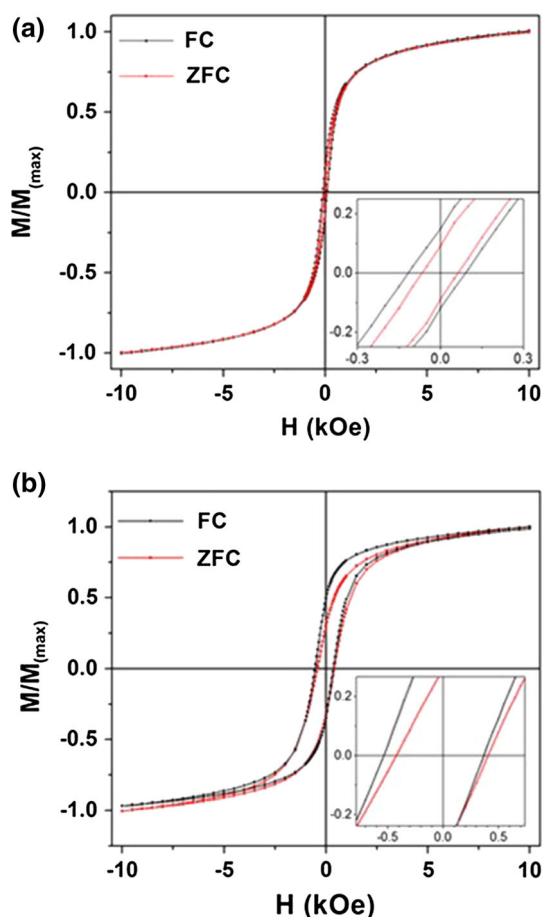
Fig. 5. Normalized magnetization $M/M_{max.}$ versus field H at 5 K for (a) as-prepared FeVO$_4$-Fe$_3$O$_4$ nanocomposites (sample A) and (b) argon annealed FeVO$_4$-Fe$_3$O$_4$ nanocomposites (Sample B). Insets showing the noticeable shift in the hysteresis curves (exchange bias). The x- and y-axis in the inset plots represent the applied field (in kOe) and normalized magnetization, respectively.
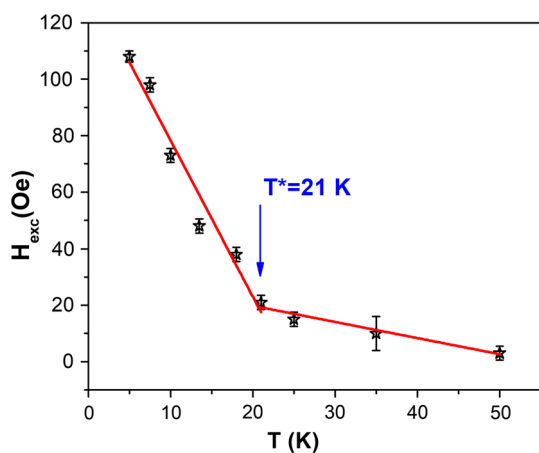

Fig. 6. Exchange Bias (H_{exc}) versus temperature (T) for argon annealed FeVO$_4$-Fe$_3$O$_4$ nanocomposites (sample B).

case of Fe/γ-Fe$_2$O$_3$ core/shell nanoparticles with the intersect signifying the freezing temperature of the core.[16] While in our case the topology is different

(see Fig. 3), we identify the intersect as the Néel temperature of an *isolated* FeVO$_4$ nanoparticle. It is thus reasonable to assume that the exchange coupling below the Néel temperature is due to the AFM transition of the entire nanoparticle, whereas in the temperature interval 22–50 K the interface FiM/AFM layer is ordered due to a *magnetic proximity* effect with thermally modified Fe$_3$O$_4$.

To confirm that EB below 50 K is, indeed, due to a coupling between FiM Fe$_3$O$_4$ and AFM FeVO$_4$, we performed a separate experiment with single-component Fe$_3$O$_4$ nanoparticle samples synthesized by the same technique and annealed under the same conditions as the composite system. The size of these Fe$_3$O$_4$ nanoparticles determined from the Scherrer formula was found to be quite similar (10 ± 2 nm) to the size of the Fe$_3$O$_4$ nanoparticles in the composite samples. EB in this single-component Fe$_3$O$_4$ was found to be practically temperature-independent between 10 K and 300 K (not shown) and of the same order of magnitude as the residual bias in the FeVO$_4$-Fe$_3$O$_4$ nanocomposites above 50 K ($\sim$ 3–4 Oe). This small residual EB generated within single component Fe$_3$O$_4$ nanoparticles is likely to be due to the known contribution of the AFM FeO phase with T_N = 190 K.[42]

To further elucidate the origin of the magnetic proximity effect in FeVO$_4$-Fe$_3$O$_4$ nanocomposites we performed XPS measurements before and after argon annealing (see Fig. 2). This allowed us to quantify the changes in the effective iron ion valency near the surface. The Fe ($2p^{3/2}$) 710 eV spectral line was reported to carry an overlap of the ferrous and ferric ions contributions.[43,44] Following the standard practice, we subtract the Shirley background from the Fe($2p^{3/2}$) peak before fitting to a dual Gaussian–Lorentzian profile.[44] By comparing the relative heights of these peaks we obtain an estimate of the Fe^{2+} versus Fe^{3+} ion contents. Our analysis reveals an increase in the relative content of ferrous ion in the composite sample upon annealing in argon, with the nominal stoichiometric ratio of Fe^{2+} to Fe^{3+} = 33:67 (approximately 1:2) for as-prepared samples changing to 46:54 (approximately 1:1) for annealed composites, which can be attributed to the appearance of oxygen vacancies. To exclude the possibility of oxygen vacancy creation in FeVO$_4$, we compared the resistivity of annealed and as-prepared composite samples. The resistivity of these samples, which is determined primarily by FeVO$_4$, would be particularly sensitive to the presence of oxygen vacancies. The measurements did not show any meaningful changes in the resistivity of the composites upon annealing, which supports our assumption that FeVO$_4$ is chemically stable at the annealing temperature of 400°C, in agreement with the previous work of Dixit et al.[32] The XPS measurements suggest that the observed magnetic proximity effect is associated with the valency modification of Fe$_3$O$_4$. While as-prepared composites have a practically ideal stoichiometric

1:2 ratio of Fe^{2+} to Fe^{3+} in Fe_3O_4 nanoparticles, upon annealing in argon the same nanoparticles become oxygen deficient, with the ratio of Fe^{2+} to Fe^{3+} close to 1. This is consistent with the reduction of at least the surface layer of Fe_3O_4, observed previously in this temperature range.[45]

Recently Ding et al.[46] reported the observations of enhanced exchange bias in the system $CoO_{1-\delta}$/(NiFe,Fe) above the Néel temperature of bulk CoO. The authors attribute this effect to the presence of oxygen vacancies in $CoO_{1-\delta}$ (the AFM component). We observed a significant increase of EB at 5 K compared to the as-prepared sample from approximately 50 Oe to 110 Oe. The estimated interfacial exchange energy $\sim 40\ \mu J/m^2$ for $FeVO_4$-Fe_3O_4 nanocomposite system, is considerably smaller compared to the typical values observed in conventional AFM/FM thin films structures. This is not surprising, however, as Fe_3O_4 nanoparticles are randomly adhered to $FeVO_4$ surfaces (see Fig. 3) and the effective contact area is estimated to be at least an order of magnitude smaller than in the former case. While some of the increase in the EB may be attributed to the increase in the area of the physical contact between nanoparticles upon annealing, the observed high blocking temperature $T_B \sim 50$ K found in the post-annealed samples, more than twice the value of the Néel temperature $T_{N1} = 22$ K in $FeVO_4$, suggests that a different mechanism is responsible for this effect. Based on the XPS measurements, we conclude that while oxygen vacancies in Fe_3O_4 are likely to be generated by thermal treatment, the oxygen content in the AFM component ($FeVO_4$) has not changed. Hence, the mechanism responsible for the enhanced blocking temperature is likely to be the proximity effect with oxygen deficient Fe_3O_4, similar to the one suggested in an earlier study.[25]

CONCLUSIONS

In conclusion, we have observed a significant increase of the exchange bias field at low temperatures in post-annealed AFM/FiM composites compared to as-prepared samples from approximately 50 Oe to 110 Oe. The blocking temperature $T_B \sim 50$ K found in post-annealed samples, has also increased by more than a factor of two, compared to the Néel temperature $T_{N1} = 22$ K of bulk $FeVO_4$, which we attribute to the magnetic proximity effect with the reduced Fe_3O_4 adjacent to $FeVO_4$. Naively, the reduction of oxygen content in Fe_3O_4 leads to the increase of the number of unpaired surface Fe^{2+} spins, which are responsible for the magnetization of magnetite; lattice mismatch and other structural effects changing the electronic, magnetic, and morphological structure of the Fe_3O_4 termination layer may also play a role.[46] These effects could result in the interfacial spins pinning, leading to an increase of the blocking temperature beyond the Néel temperature of $FeVO_4$. While the observed blocking temperature in $FeVO_4$/Fe_3O_4 composites is too low for practical applications, this nanocomposite system provides an interesting example of a more complex interfacial exchange coupling, and thus may serve as a testbed for further studies of the origin of magnetic proximity and exchange bias effects in systems with higher Néel temperatures.

REFERENCES

1. T. Jonsson, J. Mattsson, C. Djurberg, F.A. Khan, P. Nordblad, and P. Svedlindh, *Phys. Rev. Lett.* 75, 4138 (1995).
2. E. Winkler, R.D. Zysler, M.V. Mansilla, D. Fiorani, D. Rinaldi, M. Vasilakaki, and K.N. Trohidou, *Nanotechnology* 19, 185702 (2008).
3. R.J. Tackett, A.W. Bhuiya, and C.E. Botez, *Nanotechnology* 20, 445705 (2009).
4. B. Aslibeiki, P. Kameli, H. Salamati, M. Eshraghi, and T. Tahmasebi, *J. Magn. Magn. Mater.* 322, 2929 (2010).
5. S.S. Laha, R. Mukherjee, and G. Lawes, *Mater. Res. Expres* 1, 025032 (2014).
6. Q.A. Pankhurst, J. Connolly, S.K. Jones, and J.J. Dobson, *J. Phys. D Appl. Phys.* 36, R167 (2003).
7. A. Gupta and M. Gupta, *Bio Mater.* 26, 3995 (2005).
8. F. Chen, L. Zhang, Q. Chen, Y. Zhang, and Z. Zhang, *Chem. Commun.* 46, 8633 (2010).
9. H. Arora, M. Jensen, Y. Yuan, A. Wu, S. Vogt, T. Paunesku, and G. Woloschak, *Cancer Res.* 72, 769 (2012).
10. M. Arachchige, S. Laha, A. Naik, K. Lewis, R. Naik, and B. Jena, *Micron* 92, 55 (2017).
11. P. Kumar and K. Mandal, *J. Appl. Phys.* 101, 113906 (2007).
12. Q.K. Ong, A. Wei, and X. Lin, *Phys. Rev. B* 80, 134418 (2009).
13. X. Sun, N.F. Huls, A. Sigdel, and S. Sun, *Nano Lett.* 12, 246 (2011).
14. R. Das, J. Robles, M. Glassell, V. Kalappattil, M.H. Phan, and H. Srikanth, *J. Electron. Mater.* 6, 056719 (2018).
15. J. Nogués and I.K. Schuller, *J. Magn. Magn. Mater.* 192, 203 (1999).
16. M.H. Phan, J. Alonso, H. Khurshid, P. Lampen-Kelley, S. Chandra, K.S. Repa, Z. Nemati, R. Das, O. Iglesias, and H. Srikanth, *Nanomater.* 6, 221 (2016).
17. W.H. Meiklejohn and C.P. Bean, *Phys. Rev.* 102, 1413 (1956).
18. Z.M. Tian, S.L. Yuan, L. Liu, S.Y. Yin, L.C. Jia, P. Li, S.X. Huo, and J.Q. Li, *J. Phys. D Appl. Phys.* 42, 035008 (2009).
19. G. Lavorato, E. Winkler, A. Ghirri, E. Lima, D. Peddis, H.E. Troiani, D. Fiorani, E. Agostinelli, D. Rinaldi, and R.D. Zysler, *Phys. Rev. B* 94, 054432 (2016).
20. M. Feygenson, E. Formo, K. Freeman, N. Schieber, Z. Gai, and A. Rondinone, *J. Phys. Chem. C* 119, 26219 (2015).
21. P.J. Van der Zaag, Y. Ijiri, J.A. Borchers, L.F. Feiner, R.M. Wolf, J.M. Gaines, R.W. Erwin, and M.A. Verheijen, *Phys. Rev. Lett.* 84, 6102 (2000).
22. G. Salazar-Alvarez, J. Sort, S. Surinach, M.D. Baró, and J. Nogués, *JACS* 129, 9102 (2007).
23. X.Y. Lang, W.T. Zheng, and Q. Jiang, *Nanotechnol.* 18, 155701 (2007).
24. J. Borchers, R. Erwin, S. Berry, D. Lind, J. Ankner, E. Lochner, K. Shaw, and D. Hilton, *Phys. Rev. B* 51, 8276 (1995).
25. E.A. Tereshina, Z. Bao, L. Havela, S. Daniš, C. Kuebel, T. Gouder, and R. Caciuffo, *Appl. Phys. Lett.* 105, 122405 (2014).
26. P.K. Manna and S.M. Yusuf, *Phys. Rep.* 535, 61 (2014).

27. Q.K. Ong, X. Lin, and A. Wei, *J. Phys. Chem. C* 115, 2665 (2011).
28. H. Ohldag, A. Scholl, F. Nolting, E. Arenholz, S. Maat, A.T. Young, M. Carey, and J. Stöhr, *Phys. Rev. Lett.* 91, 017203 (2003).
29. M. Ali, P. Adie, C. Marrows, D. Greig, B. Hickey, and R. Stamps, *Nat. Mater.* 6, 70 (2007).
30. K. Lenz, S. Zander, and W. Kuch, *Phys. Rev. Lett.* 98, 237201 (2007).
31. M.D. Stiles and R.D. McMichael, *Phys. Rev. B* 60, 12950 (1999).
32. A. Dixit and G. Lawes, *J. Phys. Condens. Matter* 21, 456003 (2009).
33. S.S. Laha, R. Regmi, and G. Lawes, *J. Phys. D Appl. Phys.* 46, 325004 (2013).
34. L. Zhao, M.P. Wu, K.W. Yeh, and M.K. Wu, *Solid State Commun.* 151, 1728 (2011).
35. A. Dixit, B. Ramchandran, Y.K. Kuo, and G. Lawes, *IEEE Trans. Magn.* 51, 1 (2015).
36. S.S. Laha, R.J. Tackett, and G. Lawes, *Phys. B* 448, 69 (2014).
37. S.S. Laha, E. Abdelhamid, M.P. Arachchige, A. Kumar, and A. Dixit, *J. Am. Ceream. Soc.* 100, 1524 (2017).
38. Y. Long, Z. Chen, J. Duvail, Z. Zhang, and M. Wan, *Phys. B* 370, 121 (2005).
39. R. Das, J. Alonso, Z.N. Porshokouh, V. Kalappattil, D. Torres, M. Phan, E. Garaio, J. García, J.S. Llamazares, and H. Srikanth, *J. Phys. Chem. C* 120, 10086 (2016).
40. G.F. Goya, T.S. Berquo, F.C. Fonseca, and M.P. Morales, *J. Appl. Phys.* 94, 3520 (2003).
41. A.P. Malozemoff, *Phys. Rev. B* 35, 3679 (1987).
42. Z. Swiatkowska-Warkocka, K. Kawaguchi, H. Wang, Y. Katou, and N. Koshizaki, *Nanoscale Res. Lett.* 6, 1 (2011).
43. A.P. Grosvenor, B.A. Kobe, M.C. Biesinger, and N.S. McIntyre, *Surf. Interface Anal.* 36, 1564 (2004).
44. N.S. McIntyre and D.G. Zetaruk, *Anal. Chem.* 49, 1521 (1977).
45. A. Pineau, N. Kanari, and I. Gaballah, *Thermochim. Acta* 456, 75 (2007).
46. S.L. Ding, R. Wu, J.B. Fu, X. Wen, H.L. Du, S.Q. Liu, J.Z. Han, Y.C. Yang, C.S. Wang, D. Zhou, and J.B. Yang, *Appl. Phys. Lett.* 107, 172404 (2015).